Ab initio dipole surfaces, vibrationally averaged dipole moments, and infrared transition intensities for KCN and LiCN

Geert Brocks, Jonathan Tennyson,[a] and Ad van der Avoird
Instituut voor Theoretische Chemie, Universiteit Nijmegen, Toernooiveld, 6525 ED Nijmegen, The Netherlands

(Received 5 August 1983; accepted 11 October 1983)

Using the rovibrational wave functions which have been obtained from *ab initio* potentials and making analytic fits to the *ab initio* calculated dipole surfaces, we have evaluated the dipole (transition) moments of KCN and LiCN for several vibrational states (for $J = 0$ and 1). The "exact" rotational transition intensities of the *a*-type transitions in (triangular) KCN and those of (linear) LiNC and LiCN can be rather accurately reproduced by a rigid rotor model with the vibrationally averaged dipole moments; for the (weak) *b*-type transitions in KCN this model breaks down, however. Although the bending motions in these cyanides have large amplitudes, the vibrational transition intensities in LiNC and LiCN conform to the harmonic oscillator model. In KCN, where the large amplitudes of the bending modes and their coupling with the K–CN stretch leads to significant anharmonic shifts in the transition frequencies, the harmonic intensity pattern is perturbed by Fermi resonances, for instance, between the stretch fundamental and the second bending overtone. We have also calculated the lifetime for radiative decay of (metastable) LiCN into LiNC: 24 s for the ground state, much less for vibrationally excited states.

I. INTRODUCTION

Recently much progress has been made in calculating rovibrational transition frequencies for systems with one or more large amplitude vibrational modes.[1–15] These theoretically challenging systems have led to the development of new techniques to deal with the delocalized nature of their vibrational wave functions.

Experimental spectra, however, yield not only transition frequencies but also transition intensities. For rovibrational transitions in the infrared, these intensities contain information about both the potential energy and dipole surfaces. Inverting the experimental data in order to obtain these surfaces is generally too difficult. Much insight can be gained and the interpretation of experimental spectra can be facilitated by calculating these intensities from given dipole and potential energy surfaces. To our knowledge this has never been done for a floppy system where the results are potentially most rewarding because of the large area of the surface sampled and the large variations that can be expected between vibrationally averaged dipoles in different rovibrational states.

In their work on the potential energy surfaces of KCN[16] and LiCN,[17] Wormer and co-workers noted that their extended basis set SCF dipole moments could be well represented by the long-range expressions for the interactions between closed shell ions M^+ (M = K,Li) and CN^-. This suggests that the dipole surface could be fitted for these systems using a partitioning between long and short range components similar to that used successfully for alkali cyanide potential energy surfaces.[16,17]

These surfaces have several interesting features. KCN is predicted to be triangular, in agreement with microwave experiments,[18] with a low barrier of about 500 cm^{-1} at the isocyanide structure. LiCN is predicted to have a linear isocyanide structure in agreement with the analysis of a matrix isolation study[19] and with recent molecular beam microwave measurements.[20] However, the linear cyanide structure is also predicted to form a local minimum on the surface. These potential energy surfaces have been utilized in a series of calculations on the rovibrational states of KCN[9–11] and LiCN[12] which have shown that both molecules undergo large amplitude bending vibrations. In KCN tunneling through the linear barrier was found to be significant even in low lying excited vibrational states. In LiCN, both the isocyanide and cyanide minima were found to support localized vibrational states, whereas the vibrational states in the barrier region are a mixture of delocalized (free rotor) and localized states. In this work, we use the rovibrational wave functions generated in these studies to obtain vibrationally averaged dipoles and transition intensities for KCN and LiCN; to do this we fit analytic expressions to the calculated dipole surfaces of the two molecules.

The only gas phase infrared spectrum for KCN was recorded by Leroi and Klemperer.[21] They observed only one transition, at 207 ± 20 cm^{-1}, between 200 cm^{-1} and the CN stretching mode at 2158 cm^{-1}. This does not correspond with any of the fundamentals observed by Ismail *et al.*[22] in their matrix isolation study or calculated[9–11] using the surface of Wormer and Tennyson. It has been suggested that this transition corresponds to a bending overtone.[9,10] If so, why should this overtone have enhanced intensity, greater, for example, than the stretching fundamental at about 290 cm^{-1}.[9–11,22] For LiCN the only infrared data available are from matrix isolation spectra.[19] New measurements of KCN and LiCN gas phase spectra are to be expected, however.

Finally, we point out that HNC is well known as a reaction product which is metastable with respect to isomerization into HCN.[23] Whether LiCN, which is less stable than LiNC, can be observed in the same way will depend on the

[a] Current address: SERC Daresbury Laboratory, Daresbury, Warrington, WA4 4AD, Cheshire, United Kingdom.

 0021-9606/84/073223-11$02.10

half-life for spontaneous radiative decay from LiCN into LiNC. These life times are also calculated from the dipole surface.

II. DIPOLE SURFACES

We follow the previous work on the alkali cyanides in defining a coordinate system,[12] with **r** being the CN bond vector and **R** the vector connecting the ^{12}C ^{14}N center of mass with the metal ion. In body-fixed coordinates **R** is embedded along the z axis. The angle between **r** and **R** measured from carbon is θ. In body-fixed coordinates the other polar angle of **r** is ϕ which can also be used to fully embed the coordinate system, for instance in the x–z plane.[11]

In space-fixed coordinates the dipole can be written as a tensor of rank one as[24]

$$\mu_\nu^{(1)}(\mathbf{r},\mathbf{R}) = \sum_{\lambda,l} B_{\lambda,l}(r,R)\, \mathscr{Y}_{\lambda,l}^{1,\nu}(\hat{r},\hat{R}) , \tag{1}$$

where the coupled spherical harmonic is

$$\mathscr{Y}_{\lambda,l}^{1,\nu} = \sum_{\mu,m} Y_{\lambda,\mu}(\hat{r}) Y_{l,m}(\hat{R}) \langle 1\nu|\lambda l \mu m\rangle , \tag{2}$$

and the Clebsch–Gordan coefficient is conventional.[25]

Use of the triangulation relations and the property that the dipole is antisymmetric under inversion reduces Eq. (1) to

$$\mu_\nu^{(1)}(\mathbf{r},\mathbf{R}) = \sum_\lambda [B_{\lambda,\lambda-1}(r,R)\mathscr{Y}_{\lambda,\lambda-1}^{1,\nu}(\hat{r},\hat{R}) + B_{\lambda,\lambda+1}(r,R)\mathscr{Y}_{\lambda,\lambda+1}^{1,\nu}(\hat{r},\hat{R})] . \tag{3}$$

If the system is rotated so that **R** lies along the z axis and **r** in the xz plane this formula can be written in body-fixed coordinates as

$$\mu_\nu^{(1)}(\mathbf{r},\mathbf{R}) = \sum_{\lambda,l,k} B_{\lambda,l}(r,R)\mathscr{Y}_{\lambda,l}^{1,k}(\theta,0,0,0) \times D_{\nu,k}^{(1)*}(\alpha,\beta,\phi) , \tag{4}$$

where the angular functions $\mathscr{Y}_{\lambda,l}^{1,k}$ are now expressed in body-fixed angles, $D_{\nu,k}^{(1)*}$ are rotation matrix elements and (β,α) are the polar angles of **R** in the space-fixed system. Substituting the relation

$$Y_{l,m}(0,0) = \left(\frac{2l+1}{4\pi}\right)^{1/2} \delta_{m,0}$$

into Eq. (2), evaluating the Clebsch–Gordan coefficients and using Eq. (3) the expression for the dipole moment in body-fixed coordinates Eq. (4) becomes

$$\mu_\nu^{(1)}(\mathbf{r},\mathbf{R}) = \sum_k \mu_k(r,\theta,R)\, D_{\nu,k}^{(1)*}(\alpha,\beta,\phi) , \tag{5}$$

where the internal dipole moment μ_k is given by

$$\mu_0(r,\theta,R) = \sum_{\lambda=0}^{\infty} \left(\frac{4\pi}{2\lambda+1}\right)^{1/2} C_{\lambda,0}(r,R) Y_{\lambda,0}(\theta,0) , \tag{6a}$$

$$\mu_{\pm1}(r,\theta,R) = \sum_{\lambda=1}^{\infty} \left(\frac{2\pi}{2\lambda+1}\cdot\frac{(\lambda+1)!}{(\lambda-1)!}\right)^{1/2} C_{\lambda,1}(r,R) Y_{\lambda,\pm1}(\theta,0) , \tag{6b}$$

where

$$C_{\lambda,0} = \frac{(-1)^\lambda}{4\pi}(3)^{1/2}\,[(\lambda+1)^{1/2}B_{\lambda,\lambda+1} - (\lambda)^{1/2}B_{\lambda,\lambda-1}] , \tag{7}$$

$$C_{\lambda,1} = \frac{(-1)^\lambda}{4\pi}(3)^{1/2}\left(\frac{(\lambda-1)!}{(\lambda+1)!}\right)^{1/2} \times [(\lambda)^{1/2}B_{\lambda,\lambda+1} + (\lambda+1)^{1/2}B_{\lambda,\lambda-1}] . \tag{8}$$

These expressions for μ_0, μ_{+1}, and μ_{-1} can be transformed into those for μ_z, μ_x, and μ_y by replacing the spherical harmonics in Eq. (6) by Tesseral harmonics. Since the triatomic lies in the body-fixed xz plane, μ_y is zero. Expressions for the other components are

$$\mu_z(r,\theta,R) = \sum_{\lambda=0}^{\infty} C_{\lambda,0}(r,R)\, P_\lambda^0(\cos\theta) , \tag{9a}$$

$$\mu_x(r,\theta,R) = \sum_{\lambda=1}^{\infty} C_{\lambda,1}(r,R)\, P_\lambda^1(\cos\theta) , \tag{9b}$$

in terms of associated Legendre functions.[25] As all the potential energy and dynamical calculations were performed for fixed CN bond lengths r_e, we fit analytic expressions for $C_{\lambda,\nu}(r=r_e,R)$ to the *ab initio* calculated dipole surface.

As R becomes large the dominant contributions to $\boldsymbol{\mu}$ are the dipole caused by the charge separation of M^+ and CN^- and the permanent CN^- dipole of $0.2151ea_0$ with respect to its center of mass.[16] This yields a first order expression for the long range contribution to the dipole moment:

$$\mu_z^{\mathrm{LR}}(R,\theta) = eR + \mu_{\mathrm{CN}}\cos\theta , \tag{10a}$$

$$\mu_x^{\mathrm{LR}}(R,\theta) = \mu_{\mathrm{CN}}\sin\theta , \tag{10b}$$

where $-e$ is the charge of an electron.

The leading second order long range dipole is caused by induction.[16,17] However, the explicit inclusion of charge induced dipole contributions in the long range expression did not improve the resulting fits. Probably, if one wishes to include such terms with higher inverse powers of R, they should be damped at smaller R (as it was done in fitting the LiCN potential surface[17]). In our final fits these terms were omitted.

Having fixed the long-range contribution to the dipole as in Eq. (10), we define the short-range contribution by

$$\boldsymbol{\mu}^{\mathrm{SR}} = \boldsymbol{\mu} - \boldsymbol{\mu}^{\mathrm{LR}} , \tag{11}$$

$\boldsymbol{\mu}^{\mathrm{SR}}$ is then fitted. This procedure accounts for possible truncation errors in $\boldsymbol{\mu}^{\mathrm{LR}}$.

Wormer *et al.* potential energy (and dipole) calculations[16,17] were performed at Gauss–Legendre integration points in the angle θ.[26] The CN bond length was fixed at $2.186a_0$ and $R = 4.5$, 5.0 and $5.5a_0$ for KCN[16] and $R = 3.3$, 3.8, 4.3, and $4.8a_0$ for LiCN.[17]

This facilitates the computation of the coefficients in the Legendre expansion of Eq. (9), because using the orthogonality of associated Legendre functions, we can write

$$C_{\lambda,\mu}^{\mathrm{SR}}(R) = \left(\frac{2\lambda+1}{2}\right)\frac{(\lambda-\mu)!}{(\lambda+\mu)!}\int_{-1}^{1} \mu_\mu^{\mathrm{SR}}(R,u)\, P_\lambda^\mu(u)du . \tag{12}$$

An N point Gauss–Legendre integration scheme gives exact values for $C_{\lambda,\mu}^{\mathrm{SR}}$ for $\lambda = 0$ to $N-1$ for $\mu = 0$ (z component) and $\lambda = 1$ to $N-1$ for $\mu = 1$ (x component).[26]

TABLE I. Short-range fit parameters for KCN.[a]

	$\lambda=0$	$\lambda=1$	$\lambda=2$	$\lambda=3$	$\lambda=4$
$a_{\lambda,0}$	−1.039	8.606	−0.2968	1.562×10^{-5}	-1.728×10^{6}
$b_{1,\lambda,0}$	−0.060 86	−0.8974	−0.1662	1.3811	−3.701
$a_{\lambda,1}$		0.1955	-4.733×10^{-3}		
$b_{1,\lambda,1}$		−0.1811	0.3665		

[a] See Eqs. (12) and (13).

These coefficients can be expected to have approximately an exponential dependence on R, since the major short-range contributions will be the charge penetration and exchange terms due to overlap of the M^+ and CN^- charge distributions. This suggests an analytic form:

$$C^{\mathrm{SR}}_{\lambda,\mu}(R)=a_{\lambda,\mu}\exp\left(\sum_n b_{n,\lambda,\mu}R^n\right). \tag{13}$$

We first consider the KCN dipole surface, as Wormer and Tennyson performed calculations for 26 geometries in the range $R=5$ to $8a_0$ besides those necessary for Gauss–Legendre integration. These points, which are not used for fitting, allow an assessment to be made of the fits. Inclusion of five terms, $C^{\mathrm{SR}}_{0,0}$ to $C^{\mathrm{SR}}_{4,0}$ in the expansion of μ_z^{SR} and two terms $C^{\mathrm{SR}}_{1,1}$ and $C^{\mathrm{SR}}_{2,1}$ in the expansion of μ_x^{SR} and a least-squares fit for $a_{\lambda,\mu}$ and $b_{1,\lambda,\mu}$ was found to give a good representation of the calculated points. The 50 points for KCN were fitted with an average deviation of 0.38% (absolute deviation 0.019 a.u.) in μ_z and 9.4% (0.0067 a.u.) in μ_x. Maximum errors were 9.1% (0.14 a.u.) in μ_z for $R=8a_0$, $\theta=90°$ and 39% (0.029 a.u.) in μ_x for $R=4.5a_0$, $\theta=13.1°$. Fits which included explicit charge induced contributions to the long-range terms and/or an R^2 term in the exponent of Eq. (13) were found to be less satisfactory. Coefficients of higher λ terms in the expansion of μ_x change sign with R and cannot be fitted to the form of Eq. (13). But, as μ_z is at least 15 times larger than μ_x and so dominates the total dipole, a more accurate fit of μ_x seems unnecessary.

Table I lists the short-range parameters of Eq. (13) in the expression for the total dipole:

$$\mu_z(R,\theta)=eR+\mu_{\mathrm{CN}}\cos\theta+\sum_{\lambda=0}^{4}a_{\lambda,0}e^{b_{1,\lambda,0}R}P^0_\lambda(\cos\theta), \tag{14a}$$

$$\mu_x(R,\theta)=\mu_{\mathrm{CN}}\sin\theta+\sum_{\lambda=1}^{2}a_{\lambda,1}e^{b_{1,\lambda,1}R}P^1_\lambda(\cos\theta). \tag{14b}$$

The parameters of Table I do not lead to the correct asymptotic behavior as R becomes large, because not all exponents are negative; therefore this fit is expected to be accurate only in the range $R=4.5$ to $8a_0$. Figure 1 gives contour plots of the KCN dipole surface.

For KCN, the points on the dipole surface included in the fitting procedure were fitted with roughly the same accuracy as the other points. This suggests that the same fit procedure is appropriate for LiCN, where Essers *et al.* calculated only two extra points.[17] Inclusion of four terms in the expansion of μ_z^{SR} and two terms in the expansion of μ_x^{SR} gave satisfactory results: An average deviation of 0.32%

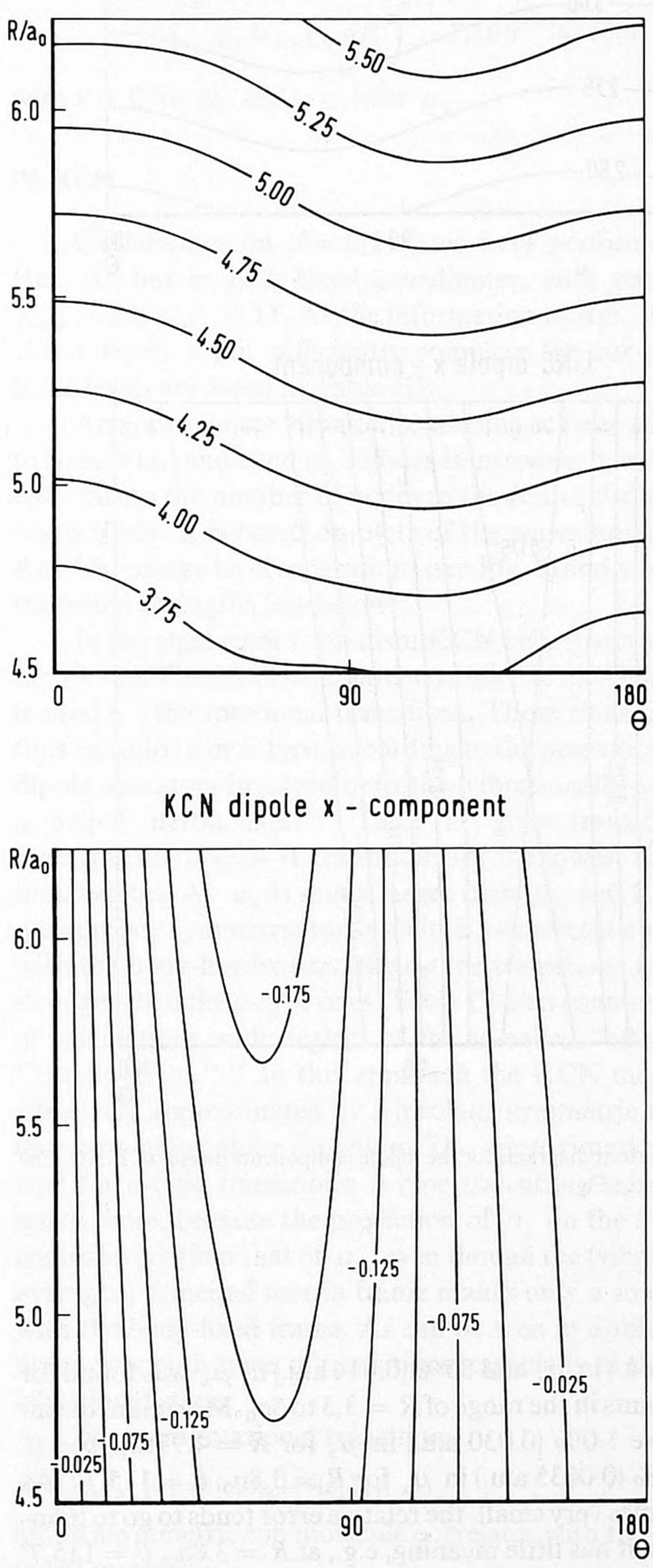

FIG. 1. Contour diagrams for the dipole components of KCN. R is the distance from the CN center of mass to K, and θ the angle **R** makes with **r**(CN), measured from C. Dipole values in ea_0.

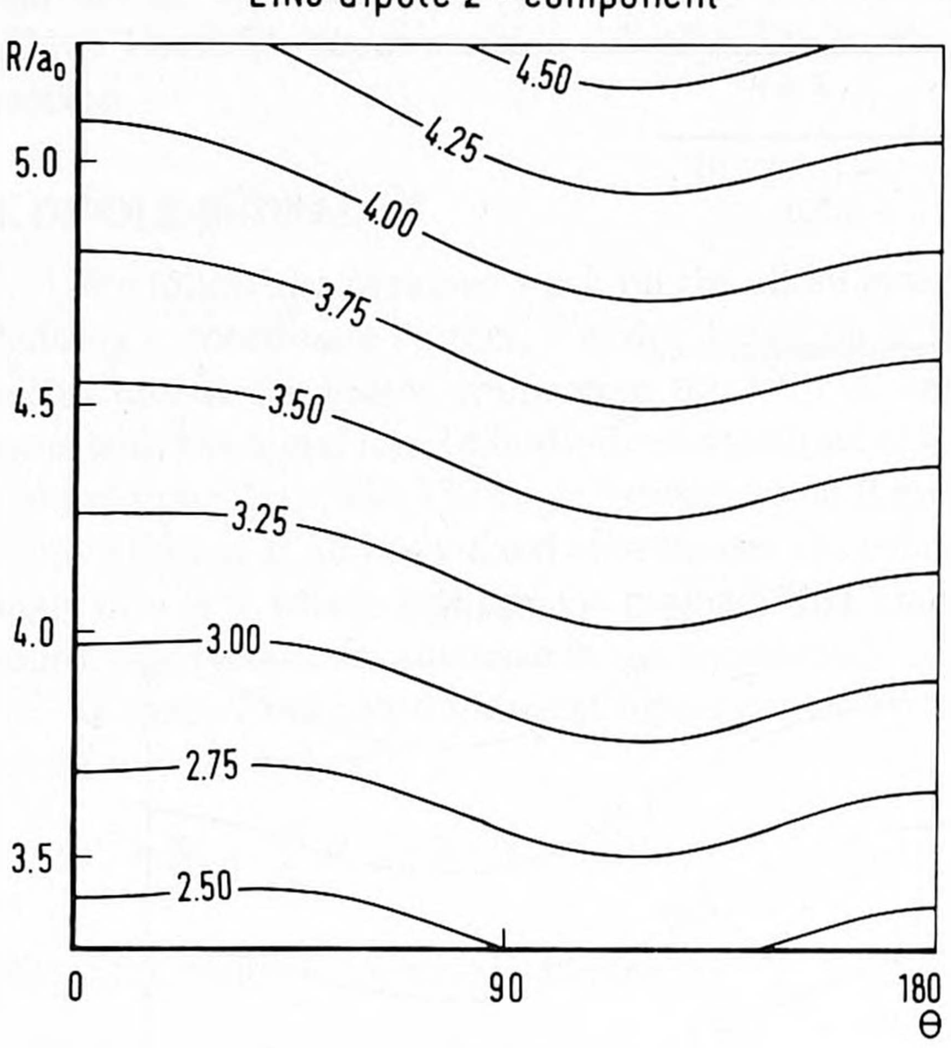

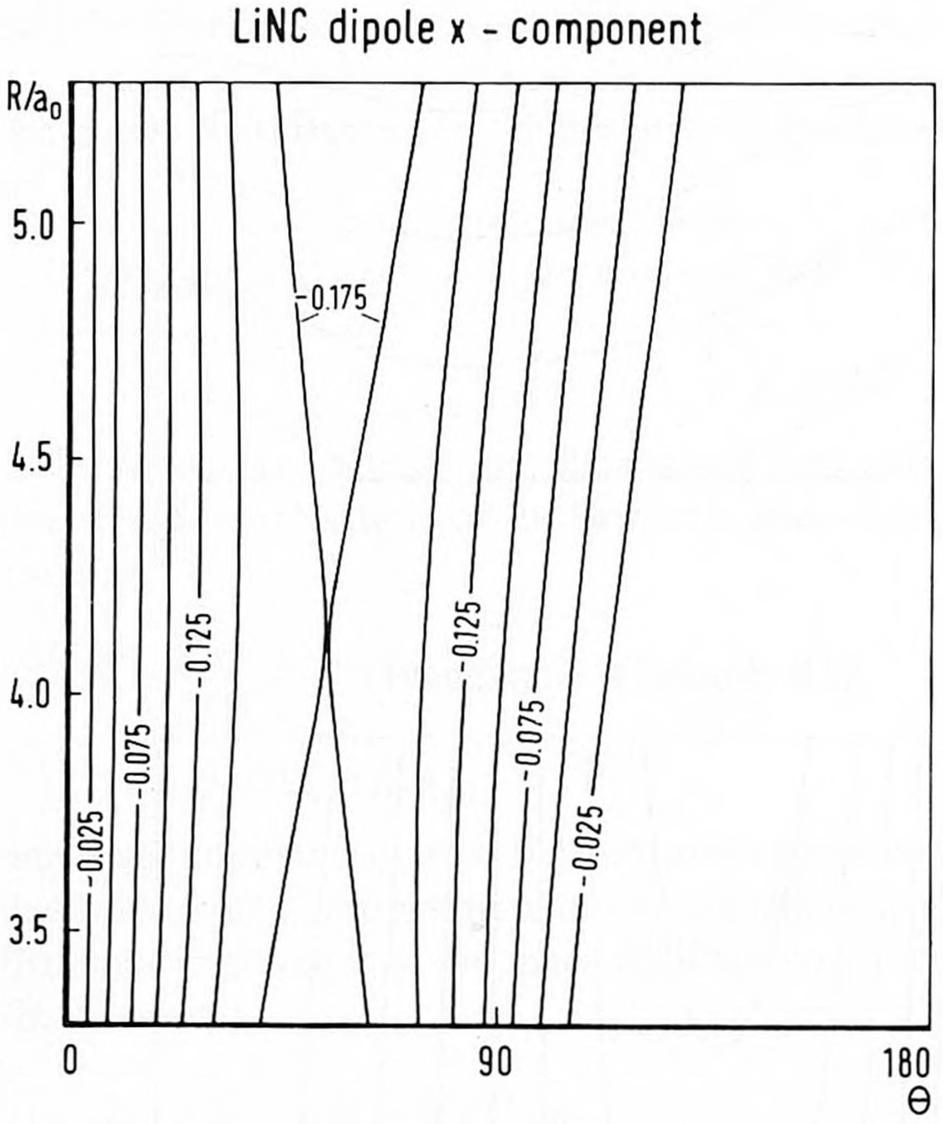

FIG. 2. Contour diagrams for the dipole components (in ea_0) of LiNC. Coordinates as in Fig. 1.

(0.0096 a.u.) in μ_z and 35% (0.014 a.u.) in μ_x was found for the 40 points in the range of $R = 3.3$ to $5a_0$. Maximum deviations were 1.0% (0.030 a.u.) in μ_z for $R = 4.975a_0$, $\theta = 0°$ and 180% (0.0035 a.u.) in μ_x for $R = 3.8a_0$, $\theta = 115.7°$. (As μ_x becomes very small, the relative error tends to go to infinity and so it has little meaning, e.g., at $R = 3.8a_0$, $\theta = 115.7°$ the SCF value for μ_x is -0.0019 a.u.). Terms up to R^2 inclusive were used in the exponent of Eq. (13). Figure 2 gives contour plots of the lithium cyanide dipole surface.

III. TRANSITION INTENSITIES, RADIATIVE DECAY, AND VIBRATIONALLY AVERAGED DIPOLE MOMENTS

The absorption coefficient for an electric dipole transition with radiation of frequency ω is given by first-order time-dependent perturbation theory as[27]

$$K(\omega) = \frac{4\pi^2}{3\hbar c}\omega\delta(\omega-\omega_{mn})\left(\frac{N_m}{g_m}-\frac{N_n}{g_n}\right)\sum_{i,j,k}|\langle\psi_{m_i}|\mu_j|\psi_{n_k}\rangle|^2, \tag{15}$$

where N_m is the density of molecules in state m (for which a Boltzmann distribution is usually assumed) and g_m the degeneracy of m. ψ_{m_i} is the wave function of a state with energy E_m, i runs over the degenerate levels of this state. ω_{mn} is the transition frequency of the transition $m\rightarrow n$: $\omega_{mn} = (E_n - E_m)/\hbar$. μ is the dipole moment operator (all in cgs units). The summation in the golden rule expression Eq. (15) is often called the transition line strength.

The coefficient of spontaneous radiative decay of state m into a lower lying state n is given in the same units as[28]

$$A_{mn} = \frac{4\omega^3}{3\hbar c^3}\sum_{i,j,k}|\langle\psi_{m_i}|\mu_j|\psi_{n_k}\rangle|^2. \tag{16}$$

So we can write for the life time of state m

$$\tau_m = \left(\sum_n A_{mn}\right)^{-1}, \tag{17}$$

where the summation is over all levels into which state m can decay.

The rovibrational calculations on KCN and LiCN by Tennyson and co-workers[10–12] used symmetrized, close-coupling type basis sets, for which the acronym LC-RAMP (linear combination of radial and angular momentum product functions) has been proposed.[15] In body-fixed coordinates, their rovibrational wave functions can be written

$$\psi^{J,M,p,v}(\alpha,\beta,\phi,R,r_e,\theta) = \sum_{k,j,n} A^{J,p,v}_{k,j,n} R^{-1}\chi_n(R)\mathcal{Y}^{J,M}_{j,k}(\alpha,\beta,\phi,\theta), \tag{18}$$

where

$$\mathcal{Y}^{J,M}_{j,k} = \frac{N_{J,j,k}}{\sqrt{2}}\left[D^{J*}_{M,k}(\alpha,\beta,\phi)P^k_j(\cos\theta) + (-1)^p D^{J*}_{M,-k}(\alpha,\beta,\phi)P_j^{-k}(\cos\theta)\right] \quad (k>0) \tag{19a}$$

$$= N_{J,j,0} D^{J*}_{M,0}(\alpha,\beta,\phi)P_j(\cos\theta), \quad (k=0), \tag{19b}$$

and

$$N_{J,j,k} = \left[\frac{1}{32\pi^3}(2J+1)(2j+1)\frac{(j-k)!}{(j+k)!}\right]^{1/2}. \tag{20}$$

In Eq. (16), J is the total angular momentum and $(J+p)$ the parity of the wave function; v numbers the vibrational levels for a given (J,M,p). P^k_j and $D^J_{M,k}$ are associated Legendre functions and rotation functions, respectively, for which the conventions of Brink and Satchler are used.[25]

From Eqs. (5)–(7), (14), and (16)–(20) the matrix elements of the dipole operator can be evaluated:

$$\langle \psi^{J,M,p,v} | \mu_\nu | \psi^{J',M',p',v'} \rangle$$
$$= (-1)^M (2J+1)^{1/2}(2J'+1)^{1/2} \begin{pmatrix} J & 1 & J' \\ -M & \nu & M' \end{pmatrix} \sum_{\nu'=-1}^{1} \sum_{\lambda,k j' j,n' n} a(jj',\lambda,\nu') b(\nu'-k) \int \chi_{n'}(R) C_{\lambda,|\nu'|}(R) \chi_n(R) dR$$
$$\times \begin{pmatrix} J & 1 & J' \\ -k & \nu' & k-\nu' \end{pmatrix} \begin{pmatrix} j & \lambda & j' \\ -k & \nu' & k-\nu' \end{pmatrix} \begin{pmatrix} j & \lambda & j' \\ 0 & 0 & 0 \end{pmatrix} \left[A^{J,p,v}_{kj,n} \cdot A^{J',p',v'}_{k-\nu' j',n'} + (-1)^{p'} A^{J,p,v}_{kj,n} \cdot A^{J',p',v'}_{\nu'-k j',n'} \right], \quad (21)$$

where

$$a(jj',\lambda,0) = [(2j'+1)(2j+1)]^{1/2},$$
$$a(jj',\lambda,1) = a(jj',\lambda,-1) = -(1/\sqrt{2})[(2j'+1)(2j+1)\lambda(\lambda+1)]^{1/2},$$
$$b(0) = 1/\sqrt{2},$$
$$b(\neq 0) = 1. \quad (22)$$

The $3j$-symbols are standard.[25] The integrals over R are calculated by an algorithm dependent on the form of the radial functions χ_n. In this case the form of LeRoy and Carley[1] is used: The χ_n are evaluated numerically on an equidistant grid in R and the radial integrals are calculated accordingly.[10,11] The indices m and n of Eq. (15) correspond to (J,p,v) and (J',p',v'), respectively; i and k run over all $(2J+1)$ and $(2J'+1)$ degenerate M and M' levels, respectively.

From Eq. (21) it can be seen that the following selection rules apply:

$$|J'-1| \leqslant J \leqslant J'+1,$$
$$\Delta J = 0 \Rightarrow \Delta p = 1,$$
$$\Delta J = 1 \Rightarrow \Delta p = 0. \quad (23)$$

In a rigid rotor formalism vibrationally averaged dipoles are found by considering pure rotational transitions and separating the rotational and vibrational matrix elements.[29,30] Because of the coupling in the basis functions via k [see Eq. (19a)], such a separation between rotational and vibrational parts is not in general possible. The $J=0$ eigenfunctions depend only on the internal coordinates, however, and $J=0$ states could be called purely vibrational [see Eqs. (18)–(20)]. An approximate rotation-vibration separation can be achieved[9] by assuming that the $J>0$ states are described by the same ($J=0$) vibrational functions, multiplied by appropriate (a)symmetric top eigenfunctions (linear combinations of $D^{J*}_{M,k}$ in general). Vibrationally averaged dipole moments can thus be defined as expectation values over $J=0$ states. Considering the basis used for expanding the wave functions, it is straightforward to compute expectation values of dipole components along the body-fixed axes used here. We find, from Eqs. (9), (18)–(20), for a given vibrational state v, that

$$\langle \mu_\nu \rangle_v = \sum_{jj',n,n',\lambda} \tfrac{1}{2}(2j'+1)^{1/2}(2j+1)^{1/2} A^{v}_{j',n'} A^{v}_{j,n} \times \int_0^\infty \chi_{n'} C_{\lambda,\nu} \chi_n \, dR \int_{-1}^{1} P_{j'}(u) P^{\nu}_{\lambda}(u) P_j(u) \, du \quad (24)$$

with $\nu = 0$ for μ_z and $\nu = 1$ for μ_x.

TABLE II. Short-range fit parameters for LiCN.[a]

	$\lambda=0$	$\lambda=1$	$\lambda=2$	$\lambda=3$
$a_{\lambda,0}$	−0.446 5	1.481×10^{-3}	−0.472 0	1.845×10^{-3}
$b_{1,\lambda,0}$	0.301 7	2.847	−1.267 8	2.024
$b_{2,\lambda,0}$	−0.034 81	−0.450 5	0.200 9	−0.2757
$a_{\lambda,1}$		0.094 28	−0.555 1	
$b_{1,\lambda,1}$		0.291 4	−0.840 1	
$b_{2,\lambda,1}$		−0.060 52	0.076 94	

[a] See Eqs. (12) and (13).

IV. KCN

Calculations on $J=0,1$ states were performed as in Ref. 10, but in body-fixed coordinates, with parameters $j_{max}=23$, $n_{max}=11$. As the information in Ref. 10 on the $J=1$ levels is not sufficiently complete for our purpose, these levels are listed in Table III.

An approximate vibrational labeling scheme according to stretch (v_s) and bend (v_b) modes is introduced, which corresponds to the number of nodes in the R and θ directions, respectively. It is based on plots of the wave functions (see Ref. 10), energy level separations (see Fig. 3) and vibrational transition strengths (see below).

In the rigid rotor formalism KCN behaves as an asymmetric top. Therefore, standard asymmetric top labeling[29,30] is used for the rotational transitions. These transitions can thus be called a or b type, according to the projections of the dipole operators involved onto the (vibrationally averaged) principal inertia axes.[9,18] Table IV gives transition line strengths for $J=0\rightarrow1$ transitions for the lowest ten vibrational states. As μ_z is much larger than μ_x and KCN is a near prolate symmetric top with its a axis almost coinciding with the body-fixed z axis, the a-type transitions are much stronger than the b-type ones. Table IV also contains results of calculations with neglect of the so-called "off-diagonal Coriolis terms."[11] In this approach the KCN molecule is effectively approximated by a (prolate) symmetric top with its a axis along the z direction. The approximation works well for a-type transitions; b-type transitions are affected much more, because the projection of μ_z on the b axis becomes larger than that of μ_x, even though the (vibrationally averaged) principal inertia frame makes only a small angle with the body-fixed frame. As can be seen in Table IV, μ_z dominates both types of transitions, especially in the higher vibrational states.

The pure rotational transition

$$(v,J_{K_a K_c}) = (v,0_{00}) \rightarrow (v,1_{11})$$

for an asymmetric top molecule correlates with the rovibrational transition

$$(2v,J_K) = (2v,0_0) \rightarrow (2v+1,1_1)$$

for a linear molecule.[31] The increase of this transition fre-

TABLE III. $J = 1$ rovibrational levels relative to the $J = 0$ levels of Ref. 10 (in cm^{-1}), using a LC-RAMP body-fixed basis set with $j_{max} = 23$ and $n_{max} = 11$. (CN bond length fixed at $2.186a_0$).

Vibrational level	Full calculation			Neglecting Coriolis terms	
	Rotational level				
(v_s, v_b)	$J_{K_aK_c} = 1_{01}$	1_{11}	1_{10}	1_{01}	$1_{11}, 1_{10}$
(0, 0)	0.2877	2.341	2.351	0.2989	2.351
(0, 1)	0.2823	2.556	2.566	0.2927	2.566
(0, 2)	0.2767	2.970	2.980	0.2863	2.980
(1, 0)	0.2822	2.800	2.811	0.2914	2.811
(0, 3)	0.2758	3.426	3.437	0.2848	3.437
(0, 4)	0.2649	6.039	6.050	0.2729	6.050
(1, 1)	0.2750	5.476	5.488	0.2823	5.488
(0, 5)	0.2601	14.66	14.67	0.2683	14.67
(0, 6)	0.2638	18.99	19.01	0.2700	19.01
(1, 2)	0.2720	18.91	18.92	0.2780	18.92

quency, shown in Table III, thus corresponds to a change of the KCN molecule from an asymmetric top to a nearly linear molecule. There is no significant change in the transition intensities, however.

In the molecular beam experiments of van Vaals *et al.*[18,20] it was not possible to obtain accurate data on relative transition intensities. For KCN it was found, however, that *a*-type transitions are much stronger than *b*-type ones. This agrees with the results of Table IV. The discrepancy of about 10% in rotational transition frequencies between *ab initio* and experimental results was analyzed by Tennyson *et al.*[9–11] It is associated with the inaccuracy of the equilibrium structure predicted by the potential surface of Wormer and Tennyson.[16]

Table V lists vibrationally averaged dipole moments along the body-fixed axes. These agree rather closely with the dipole moments for the vibrationally averaged geometries,[10] which are also shown in this table. The effect of the vibrational motion on the rotational line strengths can be deduced by comparing the "exactly" calculated results with the line strengths calculated for a rigid rotor in the vibrationally averaged geometry. The latter calculation is rather simple. Expressions for the $J = 0,1$ eigenfunctions of an asymmetric top have been given explicitly.[29,30] From these, the rotational line strengths $S(J_{K_aK_c} \rightarrow J'_{K'_aK'_c})$ for $J = 0 \rightarrow 1$ transitions of a triatomic asymmetric top can be derived:

$$S(0_{00} \rightarrow 1_{01}) = \mu_a^2 , \quad S(0_{00} \rightarrow 1_{11}) = \tfrac{1}{2}\mu_b^2 . \tag{25}$$

The position of the principal inertia axes in the vibrationally averaged geometry is easily computed, if we define the average geometry in terms of the parameters $\langle R^{-2} \rangle$ and $\langle \cos\theta \rangle$ and take the values for these parameters given by Tennyson and van der Avoird.[10] (It would be better to calculate directly the vibrationally averaged inverse inertia tensor,[9] but, for the basis used, some matrix elements are singular then.) Projecting $\langle \mu_z \rangle$ and $\langle \mu_x \rangle$ on the principal axes, gives us the rigid rotor values μ_a and μ_b.

Comparing the rigid rotor line strengths given in Table V with the exact ones in Table IV, we find good agreement for *a*-type transitions, but large differences for *b*-type transitions. The rigid rotor model predicts the *b*-type transitions by an order of magnitude too weak. So, the fact that these transitions could actually be observed in KCN,[18] is to some extent related with the large amplitude bending motions, for which it is essential to include rotation-vibration coupling. The intensities of the *b*-type transitions are dominated by the (vibrationally averaged) projection of μ_z on the *b* axis.

At low temperature only the vibrational ground state is significantly populated. Table VI gives line strengths for vibrational transitions from the ground state, accompanied by a $J = 0,1$ rotational transition. The rotational fine structure of these bands will be very complicated as the rotational constants, depending on the vibrational states, vary at least as much as the rotational line splittings. In general, μ_z will be most strongly sampled by *a*-type rovibrational transitions, so these will dominate the bands. A reasonable assumption is that the relative value of equivalent rotational transitions is a good measure for the relative intensities of the whole bands.

Three vibrational transitions are far more intense than the rest. Two of these are the bending fundamental (v_s, v_b)

TABLE IV. Transition line strengths (in a.u.) for pure rotational $J = 0 \rightarrow 1$ transitions in KCN; *a* type: $J_{K_aK_c} = 0_{00} \rightarrow 1_{01}$, *b* type: $0_{00} \rightarrow 1_{11}$.

Vibrational level	Full calculation		Neglecting Coriolis terms	
	Line strength		Line strength	
(v_s, v_b)	*a* type	*b* type	*a* type	*b* type
(0, 0)	19.42	0.0425	19.46	0.011 3
(0, 1)	19.91	0.0491	19.96	0.009 37
(0, 2)	20.43	0.0552	20.50	0.007 60
(1, 0)	20.04	0.0566	20.09	0.009 78
(0, 3)	20.57	0.0641	20.65	0.007 25
(0, 4)	21.54	0.0700	21.64	0.004 72
(1, 1)	20.76	0.0911	20.87	0.007 21
(0, 5)	21.95	0.0675	22.05	0.003 44
(0, 6)	21.74	0.0738	21.86	0.003 88
(1, 2)	21.07	0.0713	21.23	0.003 78

TABLE V. Vibrationally averaged dipole moments and rigid rotor line strengths for $J = 0 \rightarrow 1$ transitions in KCN (in a.u.). *a* type: $J_{K_aK_c} = 0_{00} \rightarrow 1_{01}$, *b* type: $0_{00} \rightarrow 1_{11}$.

Vibrational level					Rigid rotor line strength	
(v_s, v_b)	$\langle \mu_z \rangle$	$\langle \mu_x \rangle$	μ_z[a]	μ_x[a]	*a* type	*b* type
(0, 0)	4.413	−0.1056	4.409	−0.1069	19.49	0.000 029
(0, 1)	4.466	−0.0973	4.470	−0.0988	19.95	0.000 18
(0, 2)	4.527	−0.0875	4.534	−0.0903	20.50	0.000 97
(1, 0)	4.487	−0.0973	4.480	−0.1016	20.14	0.000 083
(0, 3)	4.545	−0.0853	4.550	−0.0882	20.66	0.001 2
(0, 4)	4.650	−0.0675	4.668	−0.0706	21.62	0.003 7
(1, 1)	4.568	−0.0837	4.567	−0.0882	20.87	0.001 3
(0, 5)	4.693	−0.0591	4.722	−0.0597	22.02	0.005 0
(0, 6)	4.675	−0.0645	4.705	−0.0677	21.85	0.004 1
(1, 2)	4.608	−0.0771	4.609	−0.0826	21.24	0.002 1

[a] Dipole moments in vibrationally averaged geometry (Ref. 10).

$= (0,0) \rightarrow (0,1)$ and the stretching fundamental $(v_s, v_b) = (0,0) \rightarrow (1,0)$. Especially the latter is very intense, as can be expected for a molecule consisting of two oppositely charged ions. More surprising, however, is the high intensity of the second bending overtone $(0,0) \rightarrow (0,3)$. This is due to a strong mixing (Fermi resonance) between the (1,0) and (0,3) levels. The $(v_s, v_b) = (0,0) \rightarrow (0,3)$ transition thus "steals" intensity from the stretch fundamental.[32]

Beyond the (0,3) level, the large anharmonicity of the KCN potential makes the separation between bending and stretching motions more or less arbitrary. In a harmonic picture this means that Fermi resonance effects become large, e.g., between (0,4), (1,1), and (0,5) levels. The energy level spacings, shown in Fig. 3, illustrate this point.

As we mentioned already, $J_{K_aK_c} = 1_{11}, 1_{10}$ levels correlate with the extra bending levels in a linear molecule and the effect of KCN becoming nearly linear could be studied from line splittings of higher overtones. Unfortunately, these lines are weak.

The only available low-temperature vibration spectrum of KCN is the matrix isolation spectrum of Ismail *et al.*[22] Their assignment of fundamentals was found to be in agreement with the *ab initio* results,[10] but relative intensities have not been published. An extra peak due to Fermi resonance has not been mentioned.

Next, we look at the (high-temperature) gas phase spectrum of KCN. Figure 4 shows the relative absorption coefficients for $(v_s, v_b, J = 0) \rightarrow (v_s', v_b', J = 1)$ transitions between the first ten vibrational levels at a temperature of 750 K. This spectrum is of course incomplete because at this temperature more than ten levels are significantly populated. Calculating these higher levels will be rather difficult, because it requires an enlargement of the basis set used by Tennyson and van der Avoird[15] and a corresponding increase in the cost of the dynamical calculations.

It can be seen from Fig. 4 that, due to the irregular spacings between the vibrational levels caused by the strong interaction between bend and stretch modes, transitions are relatively well separated. Many transitions are shifted significantly, as compared to the harmonic model. Several bending overtones interact with nearby stretching levels and thus pick up some intensity.

There is little experimental data available on the gas-phase spectrum of KCN. Leroi and Klemperer[21] found only one transition, at 207 cm^{-1} (gas temperatures 800 and 1000 °C). The suggestion that this transition corresponds

TABLE VI. Vibrational transitions for KCN from the ground state, accompanied by a $J = 0, 1$ rotational transition.

Vibrational level			Line strength $\times 10^2$				Line strength $\times 10^2$	
(v_s, v_b)	$J_{K_aK_c} \leftrightarrow J_{K_a'K_c'}$		→	←	$J_{K_aK_c} \leftrightarrow J_{K_a'K_c'}$		→	←
(0, 1)	0_{00}	1_{01}	0.542	0.540	0_{00}	1_{11}	0.236	0.276
(0, 1)	1_{10}	1_{11}	0.816	0.804	1_{01}	1_{10}	0.365	0.403
(0, 2)	0_{00}	1_{01}	0.002 79	0.003 06	0_{00}	1_{11}	0.008 94	0.009 35
(0, 2)	1_{10}	1_{11}	0.004 71	0.005 03	1_{01}	1_{10}	0.012 9	0.014 4
(1, 0)	0_{00}	1_{01}	0.788	0.791	0_{00}	1_{11}	0.017 9	0.014 6
(1, 0)	1_{10}	1_{11}	1.241	1.246	1_{01}	1_{10}	0.021 6	0.025 7
(0, 3)	0_{00}	1_{01}	0.442	0.444	0_{00}	1_{11}	0.006 97	0.005 24
(0, 3)	1_{10}	1_{11}	0.604	0.607	1_{01}	1_{10}	0.006 78	0.013 0
(0, 4)	0_{00}	1_{01}	0.014 8	0.015 0	0_{00}	1_{11}	0.000 525	0.000 289
(0, 4)	1_{10}	1_{11}	0.021 8	0.022 2	1_{01}	1_{10}	0.000 461	0.000 756
(1, 1)	0_{00}	1_{01}	0.007 33	0.007 44	0_{00}	1_{11}	0.000 590	0.000 447
(1, 1)	1_{10}	1_{11}	0.009 77	0.009 99	1_{01}	1_{10}	0.000 667	0.000 926

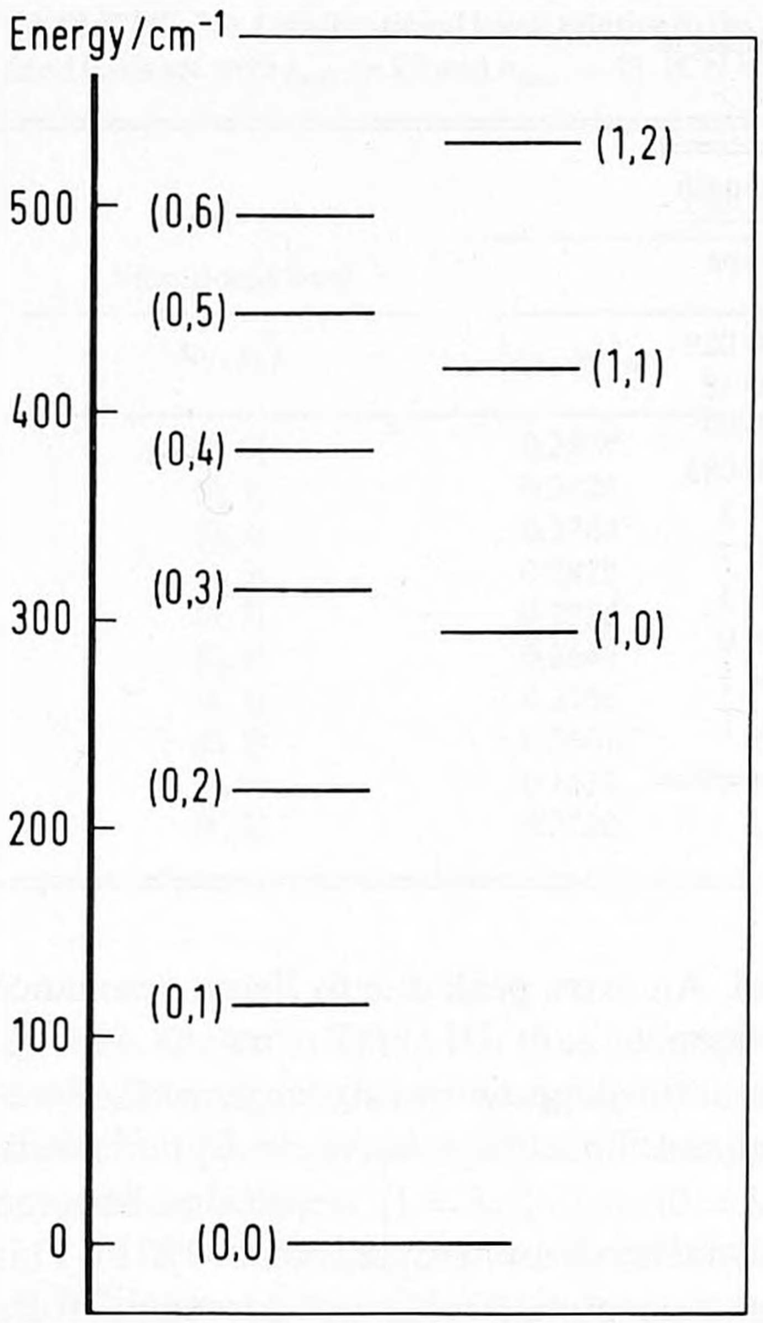

FIG. 3. KCN lowest vibrational levels as calculated by Tennyson and Van der Avoird,[10] labeled with stretch (v_s) and bend (v_b) quantum numbers.

with the second bending overtone[9,10] is made highly improbable by the results of Fig. 4. Also the CN stretch frequency of Ref. 21 does not agree with the matrix spectrum of Ismail *et al.*[22] (it lies about 100 cm^{-1} higher). Therefore, we support the suggestion of the latter authors that the "KCN spectrum" of Ref. 21 actually relates to a different molecule.

V. LiNC

According to the dynamical calculations[12] lithium cyanide behaves as a linear molecule with equilibrium LiNC (isocyanide) structure. The pure rotational spectrum is therefore much simpler than for KCN.[12,20] Table VII gives the calculated transition line strengths for $J=0\rightarrow1$ transitions and vibrationally averaged dipole moments for the lowest 10 $J=0$ states (using the $j_{max}=28$, $n_{max}=12$, $\theta_f=110°$ basis of Ref. 12). The vibrational labeling scheme is the same as used for KCN and the rotational labeling is common for a linear molecule.[12,31] As expected, the vibrationally averaged dipole along the z axis decreases with increasing bending excitation as a larger area in θ is probed and $\langle R \rangle$ decreases (see Fig. 2). Conversely, it increases with increasing stretching excitation. These effects are confirmed by comparing $\langle \mu_z \rangle$ with $\mu_z(\langle R \rangle)$ in Table VII. The vibrationally averaged dipole component along the x axis is very small indeed due to the fact that for $\theta > 90°$ long- and short-range terms have opposite sign and almost cancel. The μ_x component can practically be neglected for the transition intensities.

The effect of what is called neglect of off-diagonal Coriolis terms[11,15] is to omit all nondiagonal terms in the total angular momentum operator components J_i. In the three angle embedding of Tennyson and Sutcliffe [see Eq. (15) of Ref. 11] this implies, besides neglecting coupling terms between internal (vibrational) operators and J_i, also the neglect of nondiagonal $J_i\,J_j$ terms (i.e., in the rotational energy). In a linear molecule this results in underestimating centrifugal terms and localizing the vibrational wave function somewhat more about the linear axis, leading to a higher average dipole. The effect increases with bending excitation, since for larger deviation from the linear configuration, $J_x\,J_z$ cross terms become relatively more important (see Table VII, second column).

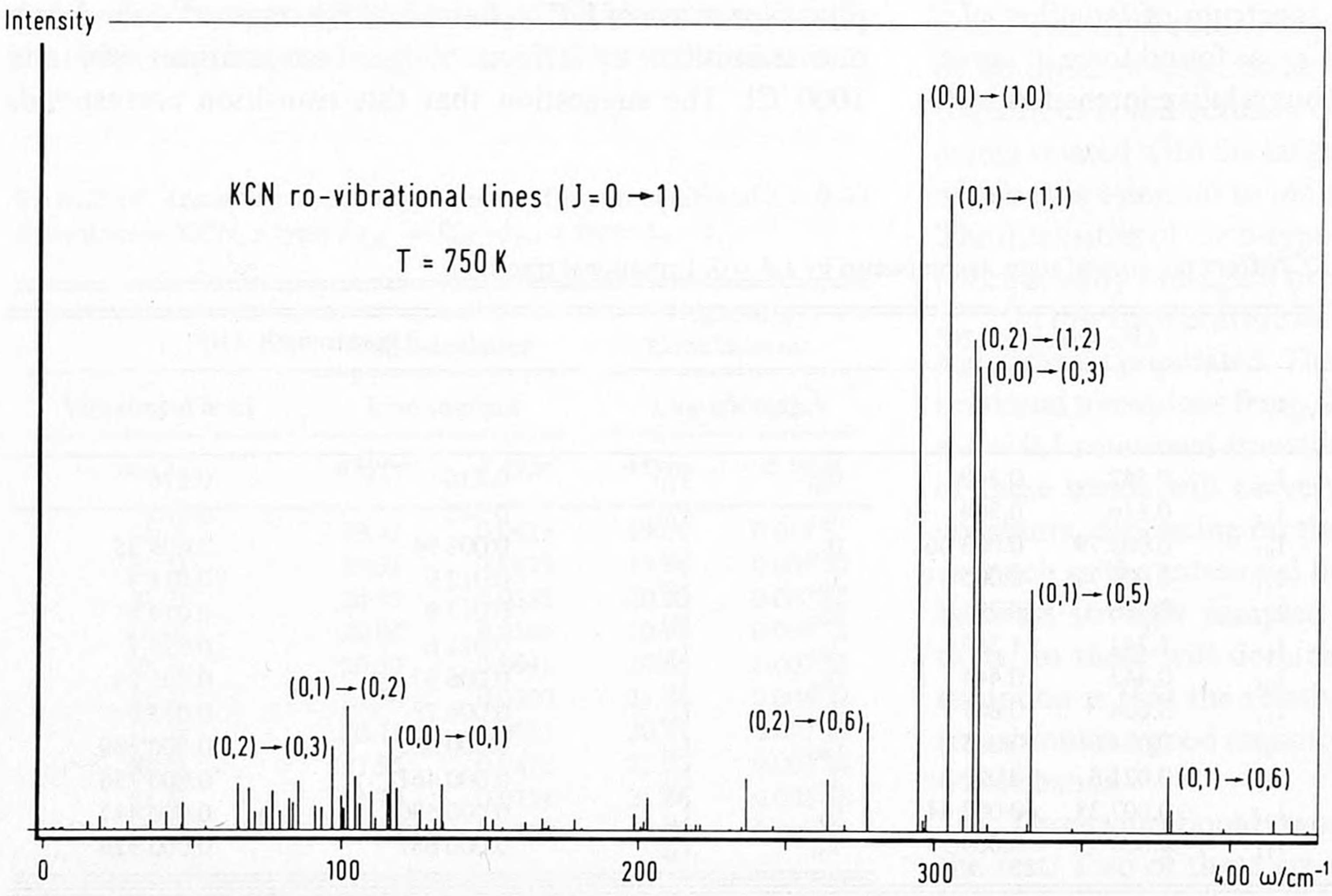

FIG. 4. Relative absorption coefficients of KCN for rovibrational $J=0\rightarrow1$ transitions between the lowest ten vibrational (v_s,v_b) levels. Energy level populations are given by the Boltzmann distribution at a temperature $T=750$ K.

TABLE VII. Line strengths for pure rotational $(J, k^p) = (0, 0^e) \rightarrow (1, 0^e)$ and transitions and vibrationally averaged dipole moments of LiNC (in a.u.).

Vibrational level (v_s, v_b)	Full	No Coriolis	Rigid rotor	$\langle \mu_z \rangle$	$\langle \mu_x \rangle$	$\mu_z(\langle R \rangle)$
(0, 0)	12.13	12.14	12.15	3.486	0.012 7	3.477
(0, 2)	11.86	11.92	11.93	3.454	0.020 3	3.425
(0, 4)	11.52	11.65	11.65	3.413	0.023 5	3.365
(0, 6)	11.09	11.30	11.30	3.362	0.023 6	3.295
(1, 0)	12.35	12.38	12.38	3.519	0.013 1	3.509
(0, 8)	10.55	10.85	10.85	3.294	0.020 1	3.209
(0, 10)	9.87	10.31	10.30	3.210	0.012 0	3.113
(1, 2)	12.07	12.15	12.16	3.487	0.020 5	3.457
(0, 12)	9.35	9.90	9.89	3.145	0.000 222	3.042
(1, 4)	11.71	11.84	11.86	3.444	0.023 3	3.393

The rigid rotor rotational line strength for a $(J_K) = (0_0) \rightarrow (1_0)$ transition for a linear molecule can easily be derived:

$$S(0_0 \rightarrow 1_0) = \mu_z^2 , \tag{26}$$

where z is the linear axis.

Taking the vibrational average $\langle \mu_z \rangle$ as the rigid rotor dipole moment, we obtain the line strengths listed in Table VII, third column. They agree quite well with the exact values of Table VII and they are practically identical to the values calculated neglecting the off-diagonal Coriolis terms. This can be understood by evaluating expressions (21) and (22) for a $J_K = 0_0 \rightarrow 1_0$ transition and making the latter approximation. This leads to an expression similar to Eq. (26), but with μ_z given by $\langle \phi_{0,0} | \mu_z | \phi_{1,0} \rangle$, where $\phi_{J,k}(R,\theta)$ is the internal part of the corresponding wave function. Since $\phi_{0,0}$ is almost identical to $\phi_{1,0}$, the observed agreement is explained.

Table VIII gives line strengths for vibrational transitions from the ground state, accompanied by a $J = 0,1$ rotational transition. Transitions are marked parallel ($\|$) for $\Delta k = 0$ and perpendicular ($\perp$) for $\Delta k = \pm 1$.[32] As can be seen from this table LiNC behaves as a perturbed harmonic oscillator. The fundamental bend and stretch transitions are by far the most intense and overtones are very weak. The energy splitting between bending overtones varies gradually by less than 10%.[12] The separation between bending and stretching modes is very clear. In spite of this behavior, the amplitudes, even in the lower lying vibrational states, are large, however, [e.g., for $(v_s,v_b,J) = (0,8,0)$ $\langle R \rangle = 4.17a_0$, $\langle \theta \rangle = 146°$] as compared to the ground state values $\langle R \rangle = 4.35a_0$, $\langle \theta \rangle = 169°$.[12]

TABLE VIII. Vibrational transitions from the ground state, accompanied by a $J = 0, 1$ rotational transition for LiNC.

$\|$ Type transition (v_s, v_b)	$(J, k^p) = (1, 0^e) \rightarrow (0, 0^e)$	$(0, 0^e) \rightarrow (1, 0^e)$
(0, 2)	0.421×10^{-3}	0.414×10^{-3}
(0, 4)	0.109×10^{-5}	0.110×10^{-5}
(0, 6)	0.970×10^{-7}	0.993×10^{-7}
(1, 0)	0.156×10^{-1}	0.160×10^{-1}
(0, 8)	0.604×10^{-8}	0.610×10^{-8}
(0, 10)	0.130×10^{-10}	0.112×10^{-10}
(1, 2)	0.244×10^{-6}	0.255×10^{-6}
$\perp$ Type transition (v_s, v_b)	$(J, k^p) = (1, 0^e) \rightarrow (1, 1^f)$	$(0, 0^e) \rightarrow (1, 1^e)$
(0, 1)	0.321×10^{-1}	0.214×10^{-1}
(0, 3)	0.531×10^{-5}	0.352×10^{-5}
(0, 5)	0.267×10^{-7}	0.179×10^{-7}
(0, 7)	0.169×10^{-8}	0.277×10^{-8}
(1, 1)	0.129×10^{-3}	0.858×10^{-4}
(0, 9)	0.201×10^{-8}	0.134×10^{-8}

Ismail *et al.* measured a matrix isolation spectrum of LiNC.[19] Again, the assignment of fundamentals is found to be in agreement with our calculations, but no relative intensities have been given.

The vibrational spectrum at higher temperature is easily understood from the previous results. Transitions with $\Delta v_b = 1$ or $\Delta v_s = 1$ are most intense, others are weak. Especially, the stretch transitions are very strong, as can be expected for an ionic molecule. As the energy spacings between higher levels decrease, the transitions between these appear on the lower frequency side of the corresponding transitions from the ground state. Because of the regularity in the spacings, the separation between corresponding transitions is not very large, however (see also Fig. 4 of Ref. 12).

VI. LiCN

A linear LiCN isomer was predicted by Brocks and Tennyson,[12] with ground state energy 2286 cm^{-1} above the LiNC ground state energy. The barrier to isomerization is at 3377 cm^{-1} above the LiNC ground state and because appreciable tunneling starts at approximately 200 cm^{-1} below the top of the barrier, the isomerization process could be observed at high temperature only.

It might be possible, however, that some chemical reactions can be found which yield the cyanide isomer LiCN as a product. Whether LiCN can actually be observed then depends on its lifetime. In a molecular beam this lifetime is probably determined by the half-lifetime for spontaneous radiative decay of LiCN into LiNC. In the gas phase collisional processes will be important as well but their effect on the LiCN lifetime will be hard to assess theoretically. Table IX gives the radiative decay life times for the lowest vibrational

TABLE IX. Half-lifetimes for LiCN vibrational states ($J = 0$), vibrationally averaged dipole moments and line strengths for rotational $(J, k^p) = (0, 0^e) \rightarrow (1, 0^e)$ transitions.

				Line strength	
(v_s, v_b)	τ (s)	$\langle \mu_z \rangle$	$\langle \mu_x \rangle$	Full	Rigid rotor
(0, 0)	24.5	3.709	−0.0430	13.75	13.76
(0, 2)	0.46	3.675	−0.0756	13.41	13.51
(0, 4)	0.80×10^{-5}	3.632	−0.0989	13.04	13.19
(1, 0)	1.07	3.736	−0.0431	13.95	13.96

($J = 0$) LiCN states (calculated with $j_{max} = 44$, $n_{max} = 15$, $\theta_f = 70°$ basis of Ref. 12.) The summation in Eq. (17) goes over all LiNC ($J = 1$) states lower in energy than the particular LiCN state considered. Table IX shows that the LiCN ground state has a sufficiently long life time for its rotation spectrum to be observed. The life time of the higher states decreases rapidly with increasing exitation level. It is unlikely, therefore, that rotation spectra for these higher levels can be measured. On the other hand, the fundamental vibrational bands from the LiCN ground state will not be strongly broadened yet and it might be possible to measure a vibrational spectrum, just as for HNC[23] (which is the metastable isomer of HCN). For the sake of completeness, Table IX gives vibrationally averaged dipole moments and rotational line strengths of LiCN (calculated with the $j_{max} = 28$, $n_{max} = 12$, $\theta_f = 40°$ basis of Ref. 12). The vibrational line strengths behave like those of LiNC: Fundamental transitions are strong, others are weak. Line strengths for the transitions $(v_s, v_b, J, k^p) = (0,0,0,0^e) \rightarrow (0,1,1,1^e)$ and $(0,0,0,0^e) \rightarrow (1,0,0,0^e)$ are 0.0277 and 0.0117 a.u., respectively.

VII. CONCLUSIONS

In this study we have performed calculations on rovibrational transition intensities for the lithium and potassium cyanides. We have used an analytical dipole surface fitted to calculated SCF dipole moments[16,17] and rovibrational wave functions from LC-RAMP calculations.[10–15]

The vibrationally averaged dipole moments follow closely the dipole moments for vibrationally averaged geometries.[10,12] The intensities of the rotational transitions calculated from these vibrationally averaged dipole moments in a rigid rotor model are compared with the results of the full calculations including the vibration-rotation coupling. For LiNC, LiCN and the *a*-type transitions in KCN they are in good agreement; for *b*-type transitions in KCN the rigid rotor model predicts the intensities too weak by an order of magnitude. For both KCN and LiNC the transition strengths are dominated by the dipole component along the body-fixed *z* axis, which in the long range is given by the charge separation.

The vibrational spectrum of KCN is not very regular in appearance, due to strong interactions between bending and stretching modes. This results in large shifts in energy levels and irregular spacings between them. In particular there is a strong Fermi resonance between the stretch fundamental and the second bending overtone, by which the latter steals considerable intensity from the first. Also, many of the higher transitions pick up some intensity by resonance effects. On the other hand, in LiNC bending and stretching motions are well separated in the lower lying vibrational levels. Fundamental transitions are by far the most intense.

A metastable LiCN molecule was predicted by Brocks and Tennyson.[12] The present results show that, if this LiCN molecule could be prepared by some chemical reaction, the ground state is sufficiently stable against spontaneous radiative decay, to be observed (half-lifetime 24.5 s).

Experimental data on vibrational transitions for these molecules is very limited yet.[18,21,22] It will be useful to try and obtain gas phase infrared spectra. In view of future experiments it is useful to make estimates of the accuracy of our predictions. The potential surfaces and the dipole surfaces for KCN and LiCN have been obtained from good quality (extended basis set) SCF-LCAO calculations.[16,17] Even though electron correlation effects are not expected to be very important for the strong (ionic) interactions in these $K^+ CN^-$ and $Li^+ CN^-$ species,[16] they may still affect rotation barriers, etc., but it is difficult to assess to what extent. The accuracy of the dipole surface can be estimated (at the SCF level) by looking at the so called basis set superposition error. For KCN it has been found[16] that this error is 6.5% in μ_z and 14.5% in μ_x of the short range dipole contributions [cf. expressions (10), (11), and (14)] near the equilibrium structure (at $R = 5.04a_0$, $\theta = 90°$), while it is 8.5% in μ_z and 17% in μ_x at a larger distance ($R = 8a_0$, $\theta = 90°$). Further errors due to the analytic fit of the potential and dipole surfaces have been indicated in detail in Refs. 16 and 17 and in Sec. II of this paper. They are such that we estimate the overall error in our dipole surface to be of the order of 10% of the short range contributions (except when the latter become very small), apart from possible electron correlation effects. Therefore, we have effectively changed the short range contributions by 10% and looked at the effect on the calculated observables. The transition strengths of the rotational transitions in KCN change by 3% and 10% for *a*- and *b*-type transitions, respectively, while the more intense vibrational transitions change by less than 4%. In LiNC a similar change alters the rotational transition strengths by about 6% and the vibrational ones by 1.3% and 14% for the stretch and bending fundamentals, respectively (which are the only strong transitions in LiNC from the ground state). The radiative lifetime of LiCN changes from 24.5 to 24.4 s. So, on the whole, we conclude that the properties of KCN and LiCN that we have calculated are not very sensitive to possible errors in the dipole surface, because they are dominated by the long range (ionic) contributions to the dipoles.

Additional inaccuracies in our results arise from the use of incomplete basis sets in the dynamical calculations of the rovibrational states.[10,12] However, we have checked that increasing j_{max} from 23 to 28 in the RAMP basis of KCN[10] causes negligible change in any of the calculated intensities (or frequencies). Although the life time of LiCN is expected to depend sensitively on the rovibrational wave functions, increasing j_{max} from 44 to 46 in the LiCN calculations, just alters this lifetime from 24.5 to 24.8 s. Thus we think that it is worth comparing our calculated data to the results of future experiments on KCN and LiCN, in order to assess the remaining uncertainty in the calculated potential surfaces. Moreover, we expect that the present calculations will be helpful in unraveling the spectra to be measured.

[1]R. J. LeRoy and J. S. Carley, Adv. Chem. Phys. **42**, 353 (1980).
[2]R. J. LeRoy and J. van Kranendonk, J. Chem. Phys. **61**, 4750 (1974).
[3]A. M. Dunker and R. G. Gordon, J. Chem. Phys. **64**, 354 (1976); **68**, 700 (1978).
[4]V. A. Istomin, N. F. Stephanov, and B. I. Zhilinskii, J. Mol. Spectrosc. **67**, 265 (1977).
[5]S. L. Holmgren, M. Waldman, and W. Klemperer, J. Chem. Phys. **67**, 4414 (1977); **69**, 1661 (1978).
[6]M. Shapiro and G. G. Balint-Kurti, J. Chem. Phys. **71**, 1461 (1979); I. F. Kidd, G. G. Balint-Kurti, and M. Shapiro, Faraday Discuss. Chem. Soc. **71**, 287 (1981).
[7]P. R. Bunker, B. M. Landsberg, and B. P. Winnewisser, J. Mol. Spectrosc. **74**, 9 (1979).
[8]A. E. Barton and B. J. Howard, Faraday Discuss. Chem. Soc. **73**, 45 (1982).
[9]J. Tennyson and B. T. Sutcliffe, Mol. Phys. **46**, 97 (1982).
[10]J. Tennyson and A. van der Avoird, J. Chem. Phys. **76**, 5710 (1982).
[11]J. Tennyson and B. T. Sutcliffe, J. Chem. Phys. **77**, 4061 (1982).
[12]G. Brocks and J. Tennyson, J. Mol. Spectrosc. **99**, 263 (1983).
[13]J. Tennyson and B. T. Sutcliffe, J. Chem. Phys. **79**, 43 (1983).
[14]J. Tennyson, Comput. Phys. Commun. **29**, 307 (1983).
[15]J. Tennyson and A. van der Avoird, J. Chem. Phys. **77**, 5664 (1982).
[16]P. E. S. Wormer and J. Tennyson, J. Chem. Phys. **75**, 1245 (1981).
[17]R. Essers, J. Tennyson, and P. E. S. Wormer, Chem. Phys. Lett. **89**, 223 (1982).
[18]T. Törring, J. P. Bekooy, W. L. Meerts, J. Hoeft, E. Tiemann, and A. Dymanus, J. Chem. Phys. **73**, 4875 (1980); J. J. van Vaals, W. L. Meerts and A. Dymanus, 34th Symposium on Molecular Spectroscopy, Columbus, Ohio, RC7 (1980); 7th Colloquium on High Resolution Spectroscopy, Reading, Mass. L6 (1981).
[19]Z. K. Ismail, R. H. Hauge, and J. L. Margrave, J. Chem. Phys. **57**, 5137 (1972).
[20]J. J. van Vaals, W. L. Meerts, and A. Dymanus, J. Chem. Phys. (submitted).
[21]G. E. Leroi and W. Klemperer, J. Chem. Phys. **35**, 774 (1961).
[22]Z. K. Ismail, R. H. Hauge, and J. L. Margrave, J. Mol. Spectrosc. **45**, 304 (1973); **54**, 402 (1975).
[23]M. J. Winter and W. J. Jones, J. Chem. Soc. Faraday Trans. **78**, 585 (1982), and references therein.
[24]P. E. S. Wormer and G. van Dijk, J. Chem. Phys. **70**, 5695 (1979).
[25]D. M. Brink and G. R. Satchler, *Angular Momentum*, 2nd ed. (Clarendon, Oxford, 1968).
[26]J. Stoer, *Einführung in die Numerisch Mathematik I* (Springer, Berlin, 1979).
[27]J. D. Poll, *Intermolecular Spectroscopy and dynamical properties of dense systems*, edited by J. van Kranendonk (North–Holland, Amsterdam, 1980).
[28]E. Merzbacher, *Quantum Mechanics* (Wiley, New York, 1961).
[29]P. R. Bunker, *Molecular Symmetry and Spectroscopy* (Academic, New York, 1979).
[30]W. Gordy and R. L. Cook, *Microwave and Molecular Spectra*, 2nd ed. (Interscience–Wiley, New York, 1970).
[31]P. R. Bunker and D. J. Howe, J. Mol. Spectrosc. **83**, 288 (1980).
[32]G. Herzberg, *Molecular Spectra and Molecular Structure* (Van Nostrand, New York, 1945), Vol. 2.